DEVELOPMENT OF OPTICAL SYSTEMS

(Final Technical Report)

Contract No. NAS8-38609 Delivery Order No. 110
The University of Alabama Account Numbers 5-33475 and 5-33477

Prepared by:
Chandra S. Vikram
Center for Applied Optics
The University of Alabama in Huntsville
Huntsville, Alabama 35899

Prepared for:
COTR: William K. Witherow
National Aeronautics and Space Administration
George C. Marshall Space Flight Center
Marshall Space Flight Center, Alabama 35812

January 1995

-C O N T E N T S-

1 INTRODUCTION

The role of holography for the material processing in space program at NASA-George C. Marshall Space Flight Center is well established. The *Fluid Experiment System* (FES) employs holography to monitor several processes in the crystal growth cell. NASA KC-135 aircraft flying in parabolic trajectory, Spacelab III mission, and the *First International Microgravity Laboratory* (IML), employed holography to monitor several processes in reduced gravity environment. *Holographic Optical Laboratory* (HOLOP) and FES are space qualified holographic systems.

Traditional holography employs one-color or wavelength. The refractive index information obtained from such holograms is valuable but not sufficient in many applications. For example, simultaneously occurring temperature and concentration variations in the cell can not be separated as such from the refractive index information. Thermocouples are intrusive and can be used at limited locations only.

In this connection, NASA/MSFC took a leading role to develop two- or multi-color holography. The idea is to store holograms at more than one wavelength. The reconstruction at different wavelengths may provide different relationships to separate different physical quantities such as temperature and concentration. Successful implementation of the technique first requires solving several scientific and technological problems. These developments are well documented. [1, 2]

Also, holographic reconstructions can be analyzed by non-traditional approaches. The reconstructed wave front can in principle be used for a number of existing and future optical techniques. Only one optical system (holographic system) is flown in space, still effectively having the advantage of several hardwares. Later, several analysis techniques (even those not yet known !) can be used. Previous holograms can also be re-analyzed to retrieve additional information. Some preliminary results with Spacelab III holograms provided exiting possibilities in this connection.[2]

Continuing on those lines, this report covers some new developments of multi-color holography and one new application of holographic reconstructions. In particular, the following aspects are covered in detail :

- **Holographic fringe contrast in two-color holography with real crystal growth experiments.** The earlier (without a test cell) work showed that the effective fringe contrast in two-color holography is different from that of traditional one-color holography. In this report a critical study in a crystal

growth test cell is presented. A particular situation with a triglycine sulfate (TGS) crystal growth in a micro gravity environment is covered in some detail. Also, the case of frequency-doubled wavelengths is particularly considered, as it provides some interesting new results.

- **Three-color holography system for fluid experiments.** This study provides a conceptual design for a three-color holographic system. Just by introducing a third laser, three two-color sets can be obtained with several possible advantages including better statistical data analysis.

- **Prospective fluid and other experiments with multi-color holography.** This study provides several possible new applications of the multi-color concept. These include reduced convection crystal growth on earth, thermo-capillary phenomena study, fiber-optic sensing, etc.

- **Speckle technique applied to the wave front of reconstructed holograms.** Using a Spacelab III hologram, it is shown that the speckle technique can be used to study the high refractive gradients near the crystal-fluid interface very effectively.

2 HOLOGRAPHIC FRINGE CONTRAST IN TWO-COLOR HOLOGRAPHY WITH REAL CRYSTAL GROWTH EXPERIMENTS

In earlier works, [1-4] we considered holographic fringe contrast effects in multi-color holography. As we know that superimposing N holograms on the same recording media, the reconstruction efficiency of each component (color) reduces to $1/N^2$ times the usual (single color) efficiency. However, considerable relief is possible [1-4] using a low (say unity) reference-to-object beam intensity ratio of each component in multi-color holography. In single color holography, a high (customarily between 3 and 10) reference to object beam intensity ratio is used. This is needed to have the exposure variation within the linear portion of the emulsion response curve. However, in multi-color holography, each component (color) hologram is added incoherently. Consequently, the effective total reference-to-object beam ratio may be high even if the individual component ratio due to each color is low. Earlier publications [1-4] considered this aspect in detail and reached interesting conclusions dealing with two- and three-color holography. Generally, the need of high reference-to-object beam intensity ratio of individual colors can be avoided. This partly relieves the reconstruction efficiency problem associated with the multiplexing.

These studies have considered the medium as non despersive. The refractive index variations due to color and/or different media were not considered as the holographic fringe contrast due to the wavelength multiplexing was the main issue. Encouraged by these results, we are extending the study here to include the refractive index changes due to the media and wavelengths. Some particular examples of common crystal growth situations are also described. Two color holography is considered but the extensions to the multi-color case is straightforward.

Let us assume that two symmetrical collimated beams illuminate the hologram recording media (see **Figure 1**). Each beam contains two colors. Let us assume that the beams are identical in geometrical path lengths. In one of the beams, the transparent test cell (such as a solution crystal growth cell) is also introduced. This beam may be called the object beam and the other as the reference beam. The exposure to the recording emulsion can be written as

$$\begin{aligned} E &= \frac{1}{2}(E_o + E_R + 2\sqrt{E_o E_R}\cos\varphi_1) \\ &+ \frac{1}{2}(E_o + E_R + 2\sqrt{E_o E_R}\cos\varphi_2) \end{aligned} \tag{1}$$

where subscripts 1 and 2 correspond to the different colors and each φ is $\varphi_o - \varphi_R$, the difference between object and reference beam phases. E_0 and E_R correspond to object and reference beam exposures. It is assumed that the exposures due to different colors are equal if the emulsion sensitivity is common, otherwise the exposures are normalized for equal response. Equation (1) can be rewritten as

$$E = E_o + E_R + \sqrt{E_o E_R}\,F \tag{2}$$

where

$$F = \cos\varphi_1 + \cos\varphi_2 \tag{3}$$

Since the optical phase is $2n\pi/\lambda$ times the geometrical path, n being the medium refractive index, we obtain the following (omitting the common paths because the phase difference between the object and the reference beams is ultimately required) for the color 1

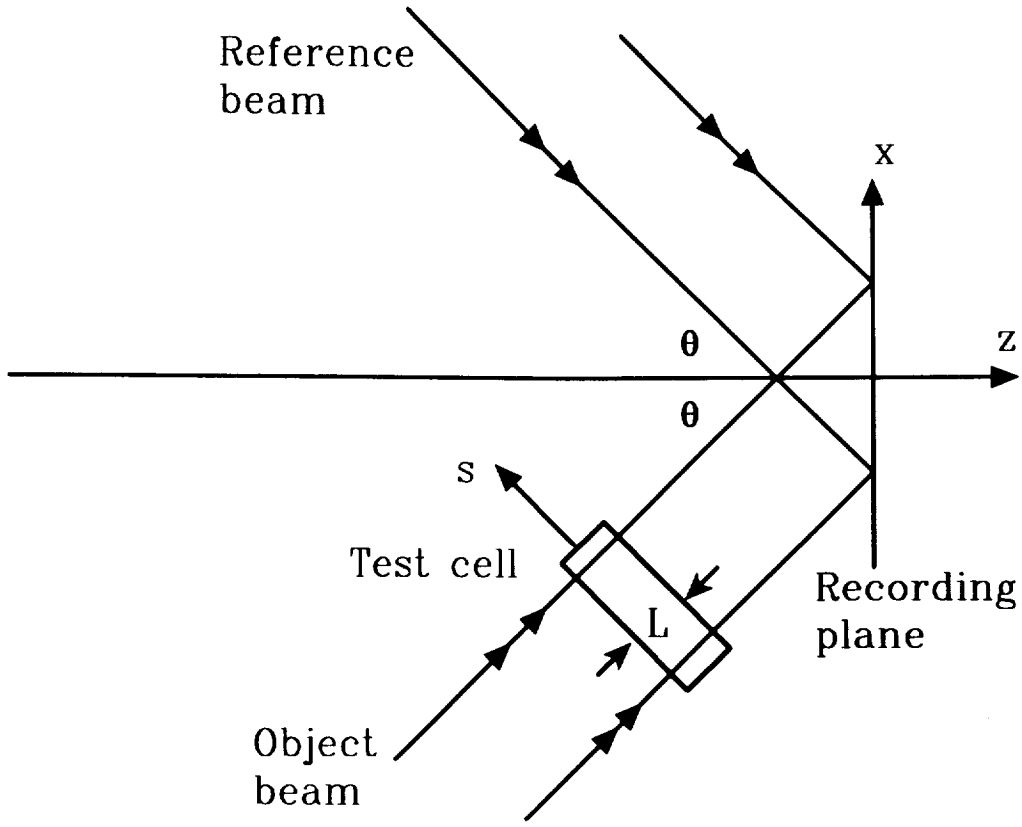

Figure 1. Diagram illustrating two-color holographic recording with object and reference beams symmetrical to the optical axis.

$$\varphi_{o1} = \frac{2\pi n_{1a} x \sin\theta}{\lambda_1} + \frac{2\pi (n_{1m} - n_{1a}) L}{\lambda_1} \tag{4}$$

and

$$\varphi_{R1} = -\frac{2\pi n_{1a} x \sin\theta}{\lambda_1} \tag{5}$$

Relationship for the color 2 can be obtained by changing the subscript 1 into 2. *a* and *m* correspond to air and medium respectively.

The last term of Equation (4) corresponds to the test cell. The phase due to the thickness L of the cell material is added and that of the air deleted. Care should be taken in assigning local values of n_{1m} . For a given x, this is the refractive index of the material at the corresponding part along the object beam direction. Coordinates x and s are related by $s = x \sin \theta$. A simple cell (rectangular parallelepiped) with the index variations only along the s - direction is considered in the study.

If the refractive index effects are omitted ($n_{1a} = n_{2a} = 1$) or the test cell is absent ($L = 0$), then in terms of the first wavelength ($\lambda = \lambda_1$) and the phase $\varphi = \varphi_1$, we have

$$F = F(\varphi) = \cos\varphi + \cos[\,(\lambda/\lambda_2)\varphi\,] \tag{6}$$

The relationship (along with extension to a third term $\cos[(\lambda/\lambda 3)\varphi\,]$ due to a third wavelength) has been extensively studied. [1-4] In the presence of the test cell and considering the refractive index effects, we obtain

$$F = F(\varphi) = \cos\varphi + \cos[\,p(\lambda/\lambda_2)\varphi\,] \tag{7}$$

where, using Equation (4), remembering that $\varphi_1 = \varphi = \varphi_{o1} - \varphi_{R1}$, and changing the subscript for the second wavelength, we obtain

$$p = \frac{2\, n_{2a}\, x \sin\theta + (n_{2m} - n_{2a})\, L}{2 n_{1a}\, x \sin\theta + (n_{1m} - n_{1a})\, L} \tag{8}$$

Notice that φ is dependent on refractive and physical properties, therefore its value in equations (6) and (7) may be different.

2.1 Refractive index of air

In this section we are summarizing some available data for the refractive index of air needed to describe a typical crystal growth situation. Although the data are not available at all the wavelengths and conditions, they are useful to describe the holographic fringe contrast situation. Using the available data [5] we have plotted the refractive index in the visible range in **Figure 2**.

Other useful data at HeNe (632.8 nm) and Ar^+ (514.5 nm) laser wavelengths for the refractive index in air against the temperature T (in degrees Celsius) are available. [6] The relationships are:

$$n_{HeNe,air} = 1 + \frac{0.292015 \times 10^{-3}}{1 + 0.368184 \times 10^{-2} T} \quad (9)$$

and

$$n_{Ar^+,air} = 1 + \frac{0.294036 \times 10^{-3}}{1 + 0.369203 \times 10^{-2} T} \quad (10)$$

In **Figure 3**, these refractive indices have been plotted near the room temperature (20 ^{o} C)

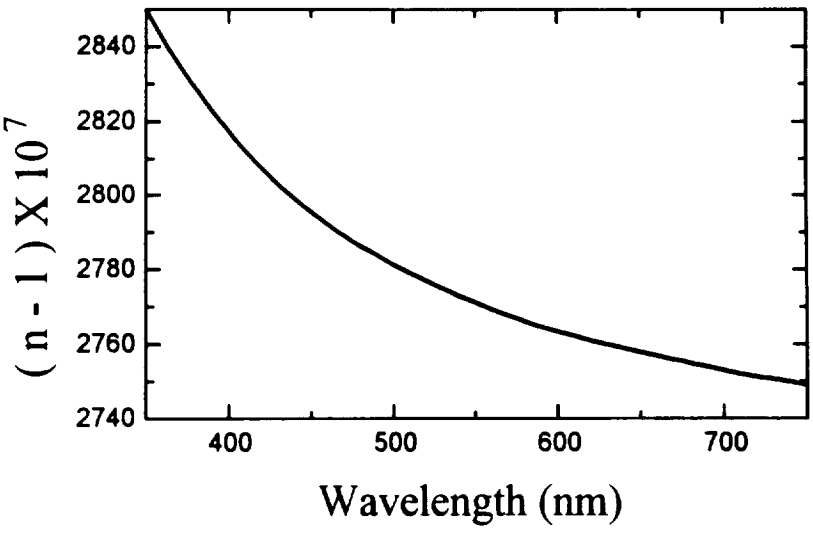

Figure 2. Plot of the refractive index of air against wavelength at 15 ^{o} C and 76 cm Hg.

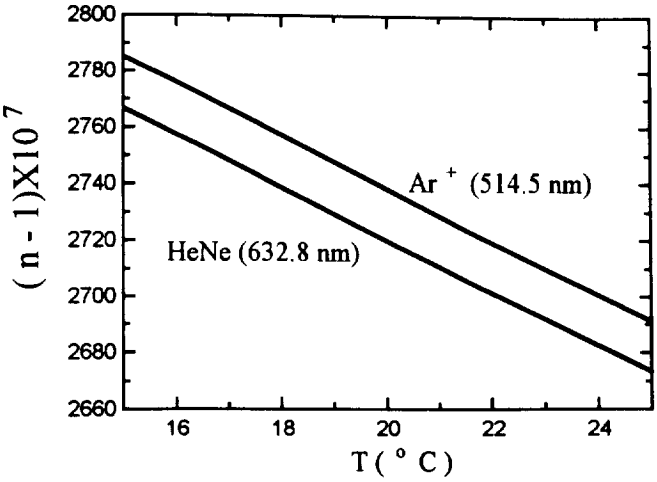

Figure 3. Variation of the refractive index against temperature for HeNe and Ar^+ lasers at particular wavelengths.

2.2 Refractive index of triglycine sulfate (TGS) aqueous solution

TGS crystal growth and subsequent analysis by holography was examined by Spacelab III mission as well as the First International Microgravity Laboratory (IML). For crystal growth, some important properties of the aqueous solution were determined by Kroes and Reiss [7] at two wavelengths (589.3 nm and 632.8 nm). From this information, some values at other wavelengths can be calculated. [2,8] At the typical crystal growth situation [9] of about 45 ° C and concentration of 513-g TGS/L H_2O, the results are (without rounding the numbers)

$$n = 1.372753 + \frac{3662.16}{\lambda^2} \tag{11}$$

$$\frac{\partial n}{\partial T} = -7.6443321 \times 10^{-4} \times \frac{n(n^2-1)}{2n^2+1} \quad {}^{\circ}C^{-1} \tag{12}$$

and

$$\frac{\partial n}{\partial c} = 3.16056467 \times 10^{-5} \times \frac{(n^2-1)(n^2+2)}{n} \quad (g\,TGS/L\,H_2O)^{-1} \tag{13}$$

where λ is in nanometers. These theoretical values are not a substitute for experimental data. However, in the absence of such information, they should be useful for modeling and preliminary system designing.

2.3 TGS aqueous solution and two-color holography with HeNe and Ar^+ lasers

As evident from equation (7), the knowledge of values of p is very important to describe the holographic fringe pattern. Now since we have sufficient information about refractive properties, the value p can be described. A careful look at our description regarding the refractive index of air reveals that at HeNe and Ar^+ wavelengths, the index information is available [**Figure 3** or equations (9) and (10)]. Since the desired data for the TGS solution is available for virtually all the wavelengths [equations (11)-(13)], this wavelength combination (632.8 nm and 514.5 nm) is ideal from the data availability point of view.

To describe the role of p on the hologram in a particular case, let us assume the following experimental situations:

- The test cell linear dimension (L) is about 2 cm. This assumption is due to the fact that critical changes around the growing crystal are generally within this length.

- The temperature in the cell is uniform at 45 ^{o} C. However, the concentration varies linearly - 513-g TGS/L H_2O at the top of the cell whereas at the bottom (near the crystal) it is 5 % less - i.e. 487.35 g TGS/L H_2O. The total change (over 2 cm distance) is thus 25.65 g TGS/ L H_2O.

- The angle between the object and the reference beams (2θ) is 45 ^{o} . That means, the hologram size for 2 cm test cell is 2 /cos (22.5^{o}) = 2.16 cm. At this stage, let us assume that the effective hologram size is 2 cm, that will be used as the size limit in our numerical analysis.

With the above assumptions, equations (11) - (13) yield the refractive index $n_{1m}(x)$ variation between x = 0 and 2 cm becomes (1 stands for HeNe laser at wavelength 632.8 nm; the unnecessary rounding of the numbers is again avoided):

$$n_{1m}(x) = 1.381898435 + 25.65 \times 8.133862154 \times 10^{-5} \times \frac{x-2}{2} \qquad (14)$$

Similarly $n_{2m}(x)$ for Ar^+ laser at 514.5 nm is :

$$n_{2m}(x) = 1.386587598 + 25.65 \times 8.249345201 \times 10^{-5} \times \frac{x-2}{2} \quad (15)$$

The resulting refractive index variations given by equations (14) and (15) are shown in **Figure 4**.

Using equations (9) and (10), we have (at the room temperature of 20 ° C) :

$$n_{1a} = 1.000271987 \quad (16)$$

and

$$n_{2a} = 1.000273817 \quad (17)$$

Now, equations (14)-(17) can be substituted into equation (8) to obtain the p - variation (at $\theta = 22.5$ ° and $l = 2$ cm). The resulting variation is shown in **Figure 5**.

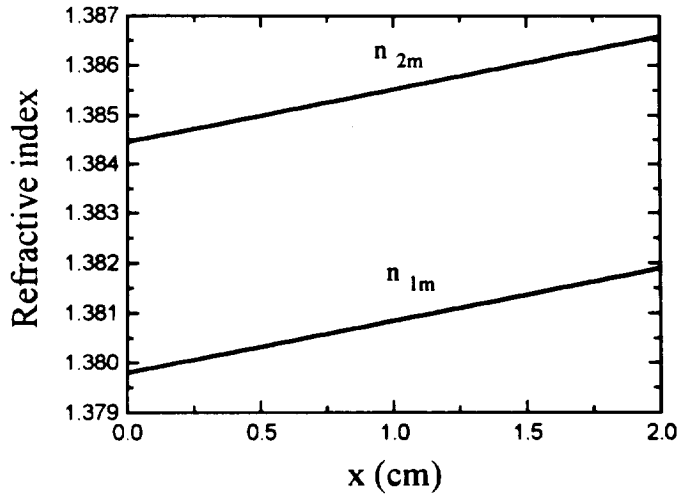

Figure 4. The refractive index variation in the TGS solution (represented against the position x in the hologram) at HeNe and Ar^+ wavelengths. The top (x = 2 cm) represents 513 g TGS/L H_2O with the linear drop in the concentration, minimum at the bottom (487.35 g TGS/L H_2O at x = 0), i.e. 5 % total drop in the concentration. Isothermal case at 45 ° C is considered.

Using p(x) variation of **Figure 5**, we have plotted some holographic fringe patterns in **Figure 6**. Dotted curves represent the situation without the test cell, i.e.

$$\varphi = \frac{4\pi n_{1a}\sin\theta}{\lambda_1} \quad ; \quad p = \frac{n_{2a}}{n_{1a}}$$

whereas the solid curve corresponds to the particular test cell considered here. As we see the fringe pattern is altered due to the concentration gradient.

These variations can be further used to study different aspects of holography. One aspect is to see the possible role in the holographic fringe contrast in a global sense.

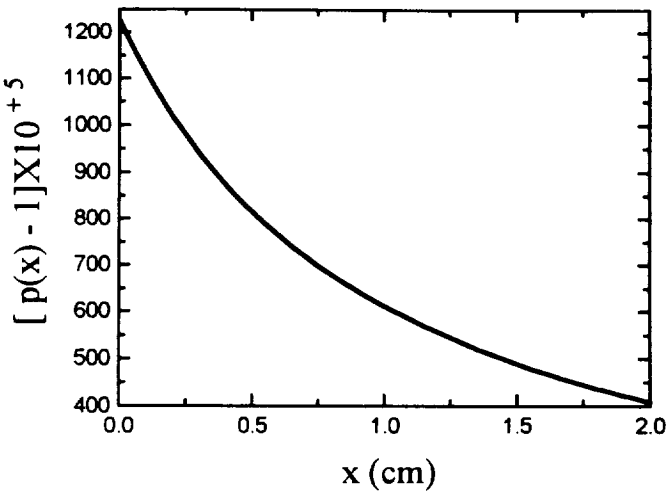

Figure 5. Variation of p(x) against x for a typical concentration situation in the TGS test cell. HeNe (632.8 nm) and Ar^+ (514.5 nm) lasers are the first and the second color respectively.

As we know F(φ) varies between + N and - N, where N is the number of colors. Let us say that this variation is between + βN and - βN, where the maximum possible value of β is unity. Now, if in a particular situation, a large portion of the hologram falls within a certain β value, we may consider the value for further quantitative applications, ignoring the portion of the hologram still with $\beta N \le |F(\varphi)|$. Some explanation about the coefficient β is appropriate here. From Equation (6), if N cosine terms are added, the maximum possible value of F(φ) will still be between + N and - N. However, due to the frequency (and/or phase) differences among the cosine terms, destructive interference will occur at

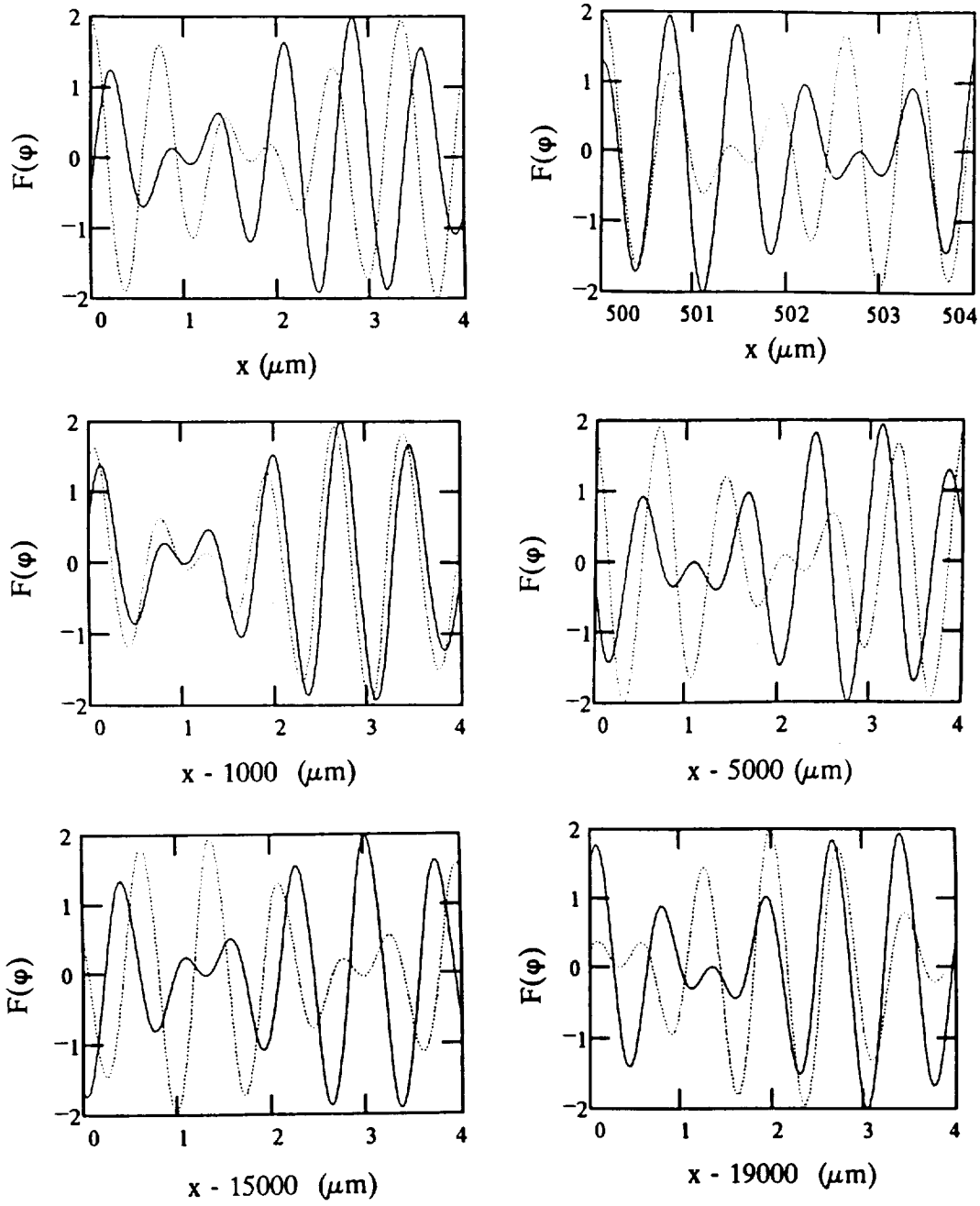

Figure 6. The holographic fringe patterns in some sections of the hologram between x = 0 and 2 cm. The dotted curve corresponds to the situation in air but without the test cell. Solid curves represent the test cell with the aqueous TGS solution and the conditions described in the text.

different locations of the hologram. The coefficient β is introduced to mathematically describe this situation so that different cases can be analytically compared.

In the following study, a large number of fringes (covering x between 0 and 200 micrometers) are studied to determine the portion of the total hologram area falling within a certain value of the coefficient β. **Figure 6** clearly shows the usefulness of such a coefficient. For example, between x = 0 and 2 μm, most of the hologram falls with $|F(\varphi)| \leq 1$ or $\beta \leq 0.5$ (because N = 2 case is being considered here). If just cos (φ) (i.e. the single-color case) is plotted, a good portion of the hologram would cover $|F(\varphi)|$ *or* $\beta \geq 0.5$. Thus, the factor β should be useful in comparing different holographic situations. We know that for a given holographic fringe contrast, the standard required reference-to-object beam intensity ratio, α, (usually between 3 and 10) and the individual ratio for each of the two colors, α′, are related by [2-4]

$$\frac{\beta\alpha'^{1/2}}{\alpha'+1} = \frac{\alpha^{1/2}}{\alpha+1} \tag{18}$$

The factor β helps distinguish various fringe contrast situations quantitatively. For example, the lowest possible value of α' = 1 and β = 0.866 yields an effective beam ratio α of 3.

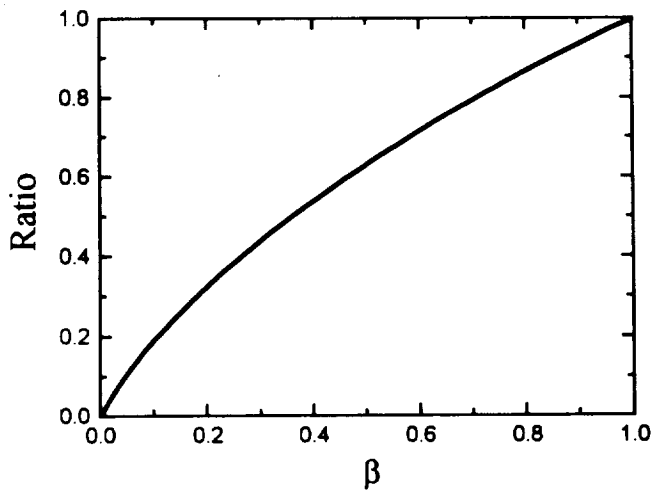

Figure 7. The fraction (ratio) of the hologram equal to or less than a certain β - value against β. The curve is for the two-color (N = 2) case and is common with or without the test cell.

For the portion within a certain β- value, the hologram fringe function F(φ) (for N = 2) was evaluated at x (in micrometers) = 0.01, 0.02, 0.03,....., 200. The number of times $|F(\varphi)| \leq \beta$ was added and divided by the total number of the countings (20001) to find the portion of the hologram within a certain β - value. The result is shown in **Figure 7**. It was found that the plot did not change by introducing the test cell and/or introducing a phase change between the two cosine components of F(φ). This is consistent with the earlier findings [3,4] that the portion is not affected by the wavelength changes or the phases, if the wavelengths are irrationally related. The factor p in equation (7) can be set equal to 1 but λ_2 replaced by λ_2/p - just equivalent to another wavelength. That is why we obtain the same β - value as that in the p = 1 case. Wavelength ratios λ/λ_2 or $\lambda/(\lambda_2/p)$ are expected to yield the same result so long as the ratios are irrational.

In the case of two-color holography with a frequency doubled laser, the hologram fringe contrast [2-4] also depends on the mutual hologram phase. The aspect may lead to interesting conclusions in the case of a real crystal growth experimental situation. This case is covered in the following section.

2.4 The case of frequency-doubled wavelengths

Earlier [1,4] we found some interesting fringe contrast and phase effects in two-color holography with a frequency-doubled-wavelength combination. In this case, the ratio and β relationship becomes dependent upon the mutual phase between the two holograms. The earlier findings did not consider the test cell or the medium refractive effects for the case of frequency doubled wavelengths . Here we describe this situation in detail.

In the case of frequency doubled wavelength combination, the fringe function F(φ) becomes

$$F(\varphi) = \cos\varphi + \cos(2p\varphi + \psi_2) \qquad (19)$$

where p characterizes the medium effects. In vacuum, p is unity and the situation is well described earlier. [1,4] In presence of a test cell with refractive index variations, p varies across the hologram. Even if there is no test cell, p is n_{2a}/n_{1a} - the ratio between the refractive indices at the second and the first wavelengths respectively in air. ψ_2 characterizes the phase difference between the holograms.

Since the role of ψ_2 is known with $p = 1$ case , let us see the situation when p changes. The relationship (19) can be written as (notice that we are dealing here the two-color, i.e. N = 2 case)

$$F(\varphi) = \cos\varphi + \cos[2\varphi + 2(p-1)\varphi + \psi_2] \qquad (20)$$

If p is nearly unity, then $2(p - 1)\varphi$ is a slowly varying function. Consequently, $2(p - 1)\varphi$ can be assumed constant over a small number of fringes. In that situation, Equation (20) resembles the usual frequency doubled case with $p = 1$ but now with a phase $\psi_2 + 2(p - 1)\varphi$ instead of the phase ψ_2 . Notice that the net effective phase is now space variant (between 0 and $2m\pi$, where m is the total number of fringes)

Theoretically, if $\varphi = 2m\pi$ and $\psi_2 = 2\pi q$ where $0 \le q \le 1$, then q becomes $q + \Delta q$ where

$$\Delta q = 2m(p-1) \qquad (21)$$

To test the hypothesis, we have plotted some fringe functions. In **Figure 8,** φ = $5000(2\pi)$ to $5001(2\pi)$ is considered to plot (for $p = 1$ and 1.00001) the portion of

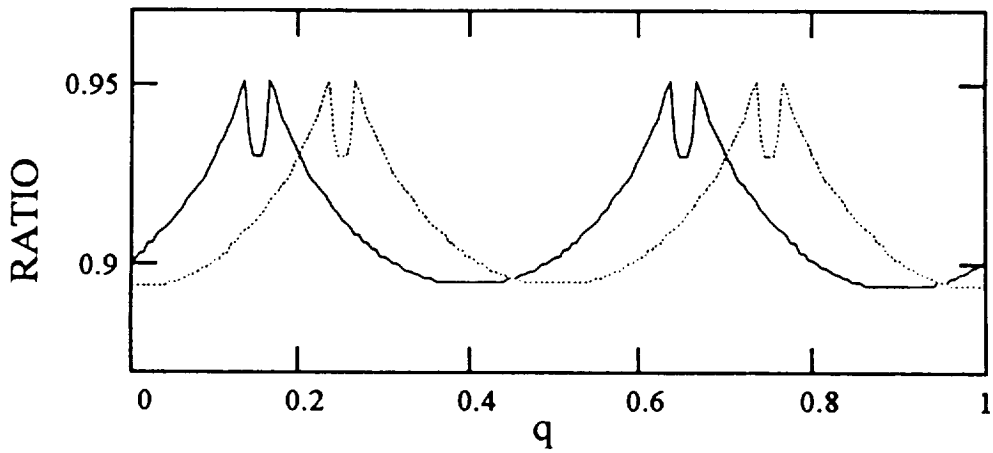

Figure 8. Fraction (ratio) of hologram below a certain β-value (0.866) against the phase factor q. m between 5000 and 5001 has been considered for the computation. The solid and the dotted curves correspond to $p = 1$ and $p = 1.00001$ cases respectively.

the hologram less than or equal to a certain β - value (0.866) against the phase $\psi_2 = 2\pi q$. The portion is actually the fraction of the values of φ corresponding to $|F(\varphi)| \leq 2\beta$. The chosen value of β yields an effective reference -to-object beam intensity ratio of 3 even if the actual beam ratio is unity. For the plot, the values of q considered were 0, 0.005, ... 1. For the computation, the function was considered in the range of m at the intervals of 0.001. We see that the plot for p = 1.00001 case has shifted back on the q - scale. In fact, the shift is precisely 0.1 as predicted by Equation (21). Since the plot for $p = 1$ case at $q = q + \Delta q$ should be the same as that for $p \neq 1$ case at q. That justifies the shift by $\Delta q = 0.1$.

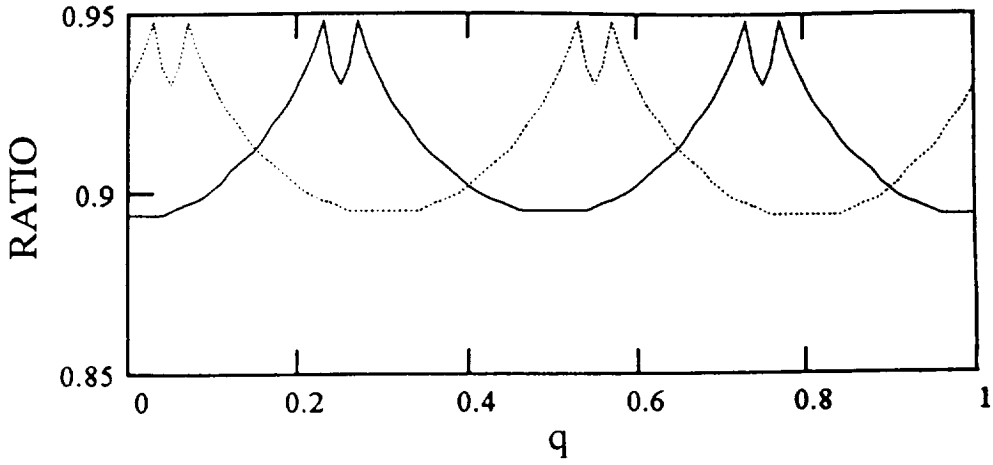

Figure 9. Same as **Figure 8** but m between 10000 and 10001 has been considered. Also, the solid and the dotted curves correspond to nonunity p (= 1.00001 presently) and unit p cases respectively.

Encouraged by this result, we used the same p (= 1.00001) but considered m between 10000 and 10001. The expected shift in q by 0.2 is evident in **Figure 9** .

Figure 10 corresponds when p = 1.004 is used with m between 10000 and 10001 . Equation (21) predicts Δq = 80. Being an integer, that means the shifted patterns should superimpose, as generally observed in the figure. For this value of p, when m between 10025 and 10026 is considered, the shift should be Δq = 80.2 or just 0.2 if the integer part is omitted. That is what we find in **Figure 11**.

So far, we plotted the curves considering a fringe. In such a small region, Δq is practically a constant. Obviously, if several fringes are considered, φ and hence Δq

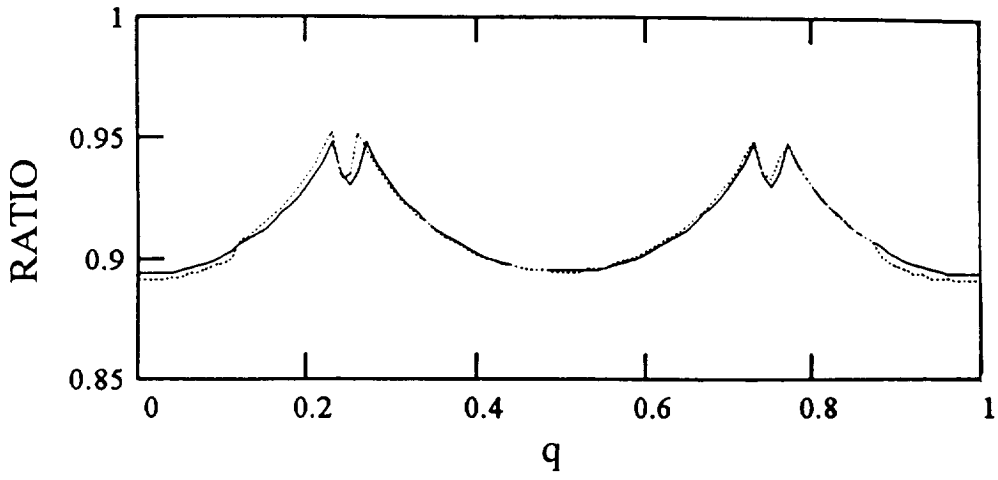

Figure 10. Same as **Figure 9** but with $p = 1.004$.

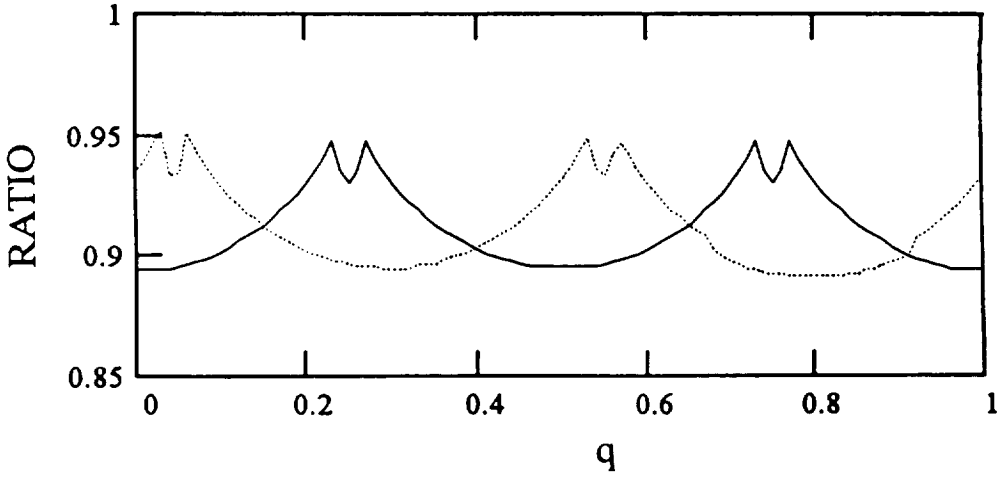

Figure 11. Same as **Figure 9** but with $p = 1.004$ and m between 10025 and 10026.

will vary depending upon the value of p . In **Figure 12**, p = 1.002 is considered with m between 10000 and 10010. According to Equation (21), Δq is between 40 and 40.04, or between 0 and 0.04 if the integral part is omitted. The shift is somewhat between this range but now the curve is changing its shape. This is because small but still some variation in Δq .

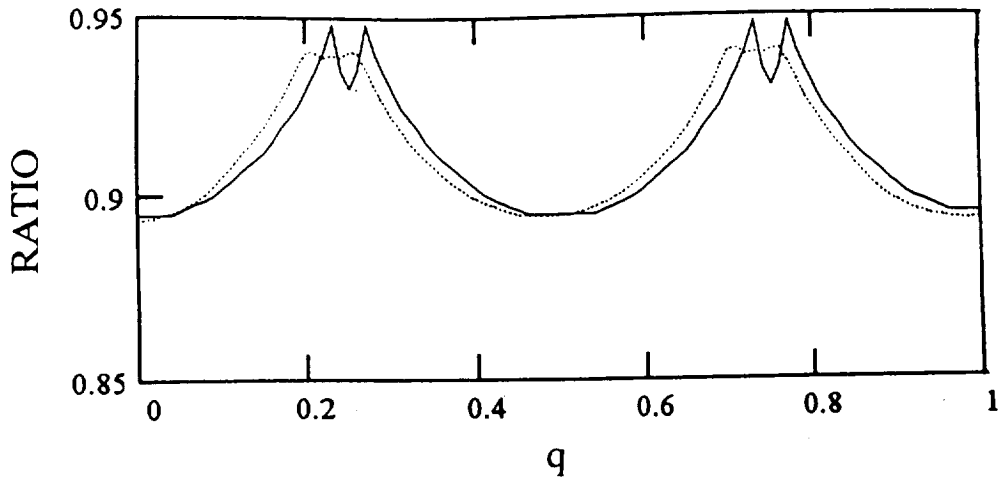

Figure 12. Same as **Figure 9** but with p = 1.002 and m between 10000 and 10010.

In **Figure 13**, the range of m is the same as that in **Figure 12** (between 10000 and 10010) but now with p = 1.02. Δq should now be between 400 and 400.4. The variation of 0.4 in Δq is large enough to smooth the curve.

An interesting question arises about Δq due to the air refractive index alone in the case of no test cell or crystal growth. The refractive indices of air at 15° C and 76 cm Hg at 350 nm and 700 nm wavelengths are 1.0002850 and 1.0002753 respectively (see **Figure 3**). Considering 700 nm and 350 nm as the first and the second wavelengths respectively, p (= n_{2a}/n_{1a}) becomes 0.999990302 or | 1 - p | as 0.000009697. Even for 10000 fringes, the change in Δq of Equation (21) becomes about 0.2 - good enough to see some averaging effect. Thus if the advantage of the phase control in the frequency doubled holography is desired, it is possible with small hologram apertures only.

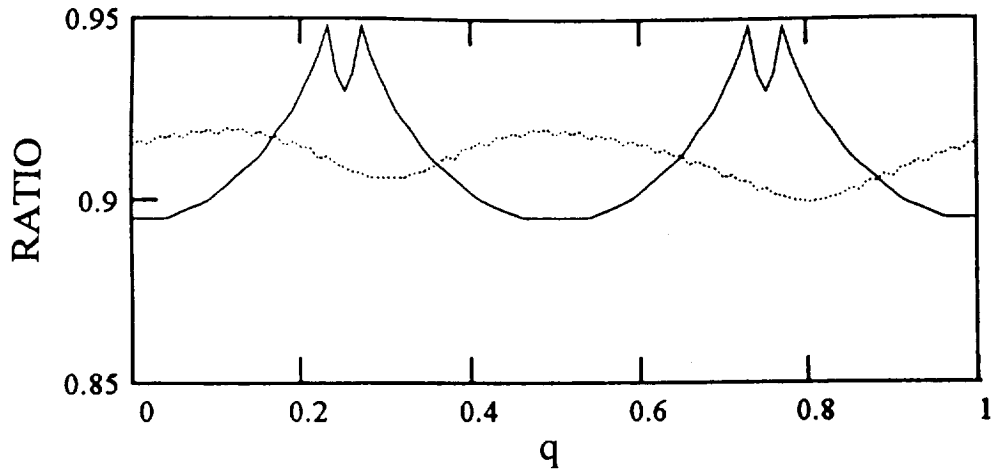

Figure 13. Same as **Figure 12** but with $p = 1.02$.

3 THREE COLOR HOLOGRAPHIC SYSTEM FOR FLUID EXPERIMENTS

As noticed earlier in this ATD (Advanced Technology Development),[1, 2] three- or multi-color holography may have several advantages over one two-color set. Basically, three two-color sets are obtained from a three-color hologram. This is possible just by introducing an additional laser to the typical two-color set. Once two-color holography is perfected, then introducing a third color is a rather simple task. After introducing the third laser, basically the hologram recording parameters are to be re-adjusted for optimum reconstruction. The analysis of each of three two-color sets can be performed the way done now with two-color holography.

MetroLaser, Irvine, California has assembled a fiber-optic two-color holography breadboard in this ATD project. The system employs a frequency-doubled YAG laser (wavelength 532 nm) and a diode laser (wavelength 680 nm). One possibility of a third wavelength is between the two wavelengths. The ideal would be at or around the middle wavelength of 606 nm - such as a Neodymium: YAG Raman laser at 602 nm. However, from a cost and practical point of view, a more common laser such as a HeNe at 632.8 nm seems to be appropriate still providing enough wavelength differences.

A wavelength lower than 532 nm can also be chosen. In fact, this will provide a larger wavelength range preferred for linearly independent interferogram relationships. HeCd laser at wavelength of 441.6 nm has been used earlier with

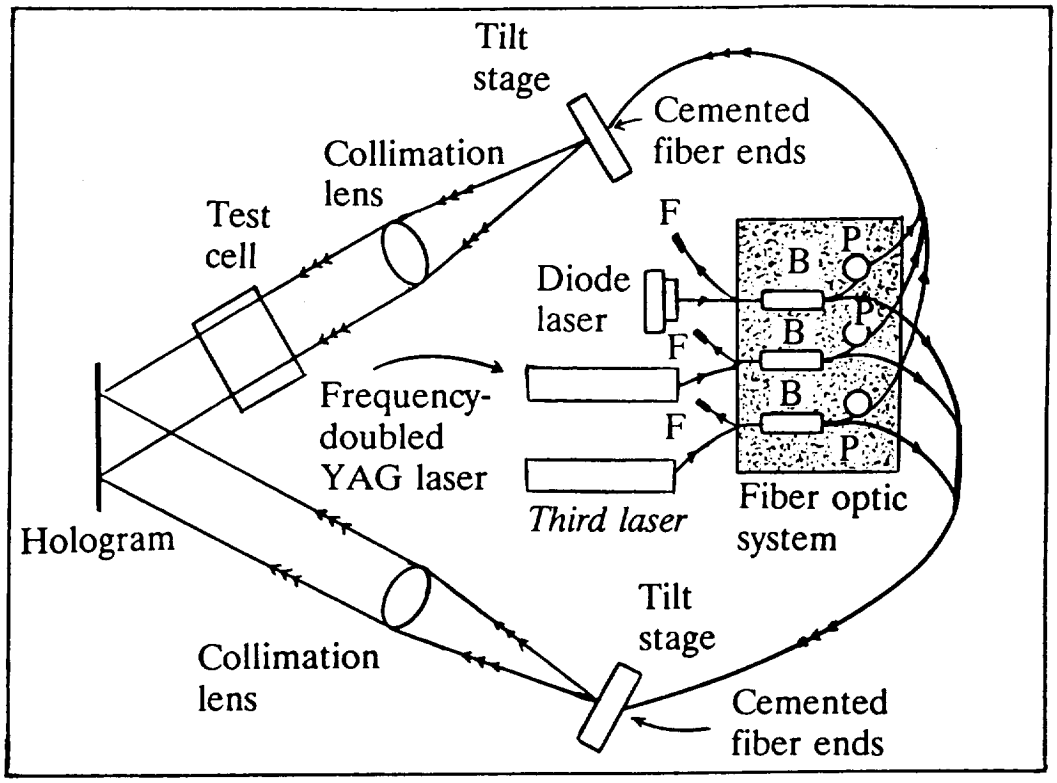

F - Feedback control signal

P - PZT Phase controller

B - Beam splitting coupler

Figure 14. Schematic diagram for three-color holography of fluids experiments. Basically a third laser is added to the existing breadboard of two-color holography with a diode laser and a frequency doubled YAG laser.

several two-color holography experiments. Addition of this provides enough wavelength difference to the 532 nm - 680 nm combination.

The schematic diagram of the three-color recording system is shown in **Figure 14**. The existing fiber optic assembly can be modified for the additional laser.

4 PROSPECTIVE FLUID AND OTHER EXPERIMENTS WITH MULTI-COLOR HOLOGRAPHY

By now it is clear that single-color interferometry of transparent media yields refractive index variations. As such it is not possible to separate simultaneously occurring temperature and concentration variations. Thus, any current and future space flight experiment will benefit by multi-color interferometry. In fact, just introducing more laser(s) in the existing set-up can be a simple starting point. Crystal growth experiments generally involve temperature and concentration variations, and materials for the use of multi-color interferometry can include, but not limited to, LAP, Urea, NH_4Cl, TGS, SCN, Protein, KDP, and ADP.

Besides these obvious applications, we have found two unique possible uses of multi-color holography. One such application is *reduced convection crystal growth on earth.* The second is *thermo-capillary phenomena study.* Some *general applications* are also described.All these applications are based on literature and discussions with other researchers.

4.1 Reduced convection crystal growth on earth

The stated advantage of crystal growth in micro-gravity situations is that only diffusion is present in the crystal growth cell. On earth, due to gravity, there is convection resulting in plumes, turbulence, etc. in the cell affecting the quality of the crystal. The main purpose of the space flight crystal growth experiments is to avoid this turbulence. However, if turbulence can be avoided here on earth, there will be considerable economic advantages. The following idea was suggested by William K. Witherow of NASA/MSFC which can open a new door in the field of crystal growth.

As we know, around the crystal in the growth cell the solution becomes diluted as the result of the crystallization. A plume like structure is formed above the crystal. In the unit-gravity situation, convection results due to solution density variations. However a reduced temperature around (but reasonably away from the interface so that the crystallization process itself is not disturbed) the crystal can increase the density to balance the material loss during the crystallization. This will reduce the convection and the need of the crystal growth in space. Obviously, a lot of

modeling and experimentation is needed to test and validate the idea. Two-color interferometry can play a key role in this , as there will be a critical need of continuous monitoring of simultaneously occurring temperature and concentration variations.

4.2 Thermo-capillary phenomena study

R. Shankar Subramanian of Clarkson University, N.Y. suggested this novel application of two-color interferometry. According to him, when a drop of liquid moves in a liquid bath due to temperature variations and due to simultaneous dissolution, the complex phenomena is ideally suited to be studied by two-color interferometry. Since a very small region around the droplet is to be studied, a truly non-intrusive approach like interferometry is needed.

4.3 Other applications

Two-color interferometry facilitates obtaining two independent relationships when two unknowns exist. Temperature and concentration variations in a crystal growth cell is one such example. However, in the literature, we have found other applications of two-color holography :

- *Study on the solidification of a binary alloy around a horizontal pipe.* [10] Two-wavelength holographic interferometry is used.
- *Simultaneous independent magnetic field and temperature measurement.*[11] Optical interferometry is used.
- *Fiber-optic interferometry.*[12] In certain fiber optic interferometry, the temperature induced changes are unwanted. Then one may propose using two wavelengths to eliminate the temperature effects.

5 SPECKLE TECHNIQUE APPLIED TO THE WAVE FRONT OF RECONSTRUCTED HOLOGRAMS

Standard interferometry is commonly used for the analysis of holograms. However, this mode is not always fruitful. For example, it is extremely difficult if high refractive index gradients are present resulting in high density fringes. In an earlier work,[2] two approaches (deflectometry using a Ronchi grating, and confocal optical processing) were demonstrated using Spacelab III mission holograms. It was found that enhanced information and/or simple analysis is possible. In the present work we demonstrate the use of a laser speckle technique

to study the reconstructed wave front. A high gradient (near the crystal-fluid interface) situation from Spacelab III mission holograms is used.

The speckle technique has wide applicability with transparent media [13] and the interest is growing. [14, 15] Obviously, several modes of the analysis are possible. One particular mode we have used for our demonstration is the rotation of laser speckles by a diffused object (ground glass) when the orientation of the incident laser beam changes. [16] The hologram of the deflecting medium (such as a crystal growth test cell) will reconstruct the deflected wave front (see for example, Figure 8 of Reference 2). When this (deflected) reconstructed wave front illuminates a ground glass, the speckles are formed in space. The objective laser speckles in a plane (called the observation plane) can be observed by a high f/number imaging system and suitable magnification as shown in **Figure 15**.

Now, for a high gradient situation, if the hologram is moved in its plane, a local region in the ground glass will be illuminated at a different angle resulting in scattered speckles rotated by the same angle. The amount of shift of the speckles in the observation plane will be the distance between the observation and ground glass planes multiplied by the angle change. Thus, a variable sensitivity approach is available.

One can observe the speckle shift while shifting the hologram. Digital analysis of the shift using a computer is possible. However, for our demonstration, image intensity subtraction using a computer has been used. The regions where the speckles are unchanged (no refractive index gradient change in the original test cell) when subtraction will show minimum or zero intensity. However, in the regions where the speckles have moved, the high contrast speckles will still be present even after the subtraction because the complete overlap of the intensities is not present.

Figure 16 shows the results obtained from a Spacelab III hologram (2PO85). The ground glass was kept 30 cm away from the hologram. The speckle pattern at 8 cm away from the ground glass was observed using a f/22 lens, CCD (demagnification on CCD about 3.5) and monitor combination. Also, a frame grabber and computer

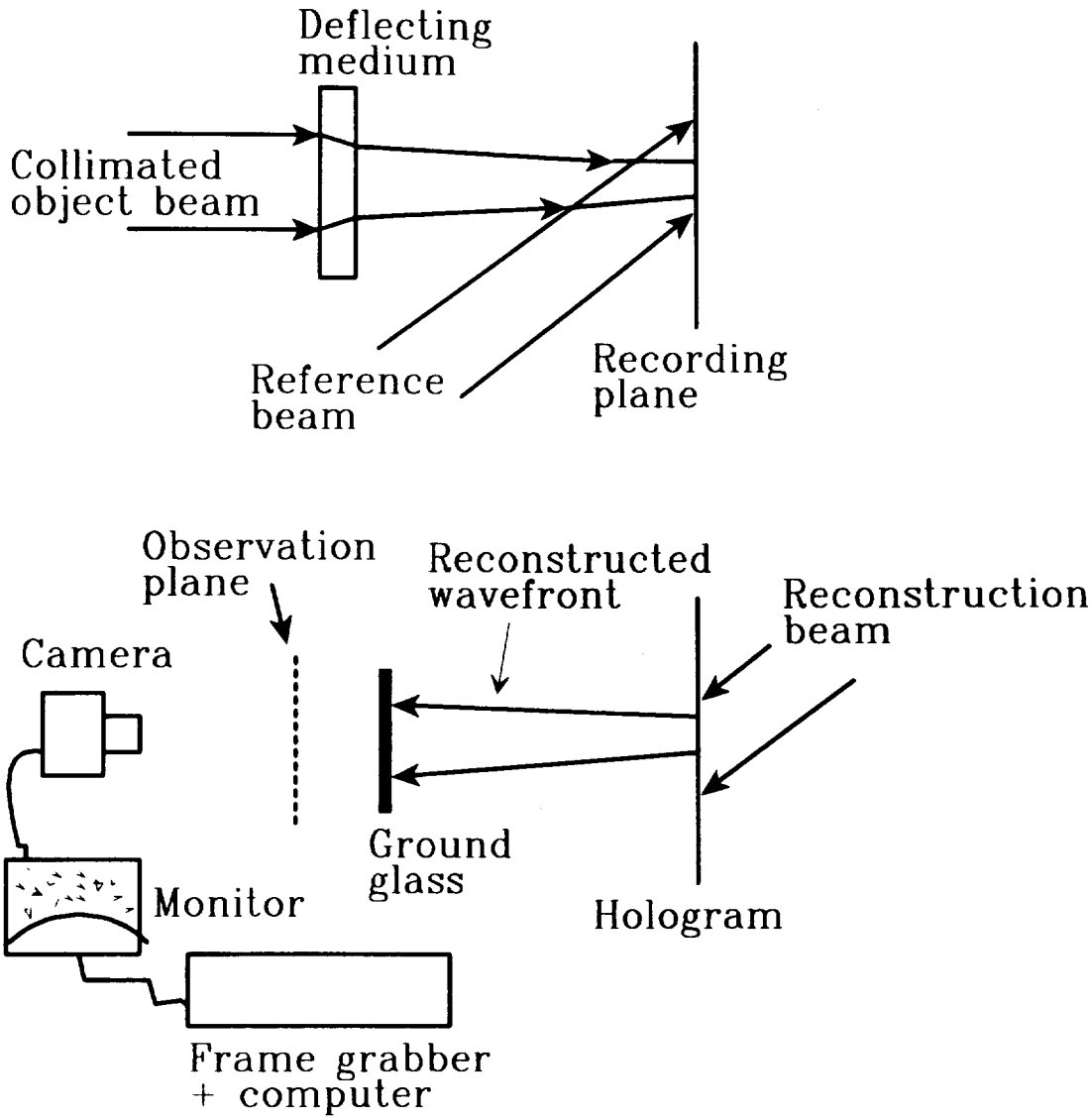

Figure 15. Reconstruction of a hologram of a deflecting medium and subsequent readout of the reconstruction using the speckle correlation method.

were used for the image substation. **Figure 16(a)** shows the original speckle pattern whereas **Figure 16(b)** is when the hologram is moved down by 0.1 mm. One may see the shifts with some care. However, **Figure 16(c),** which is the subtraction between cases **(b)** and **(c),** shows the change easily. Near the crystal surface , the refractive index gradient change was relatively severe. Therefore in that region, two speckle

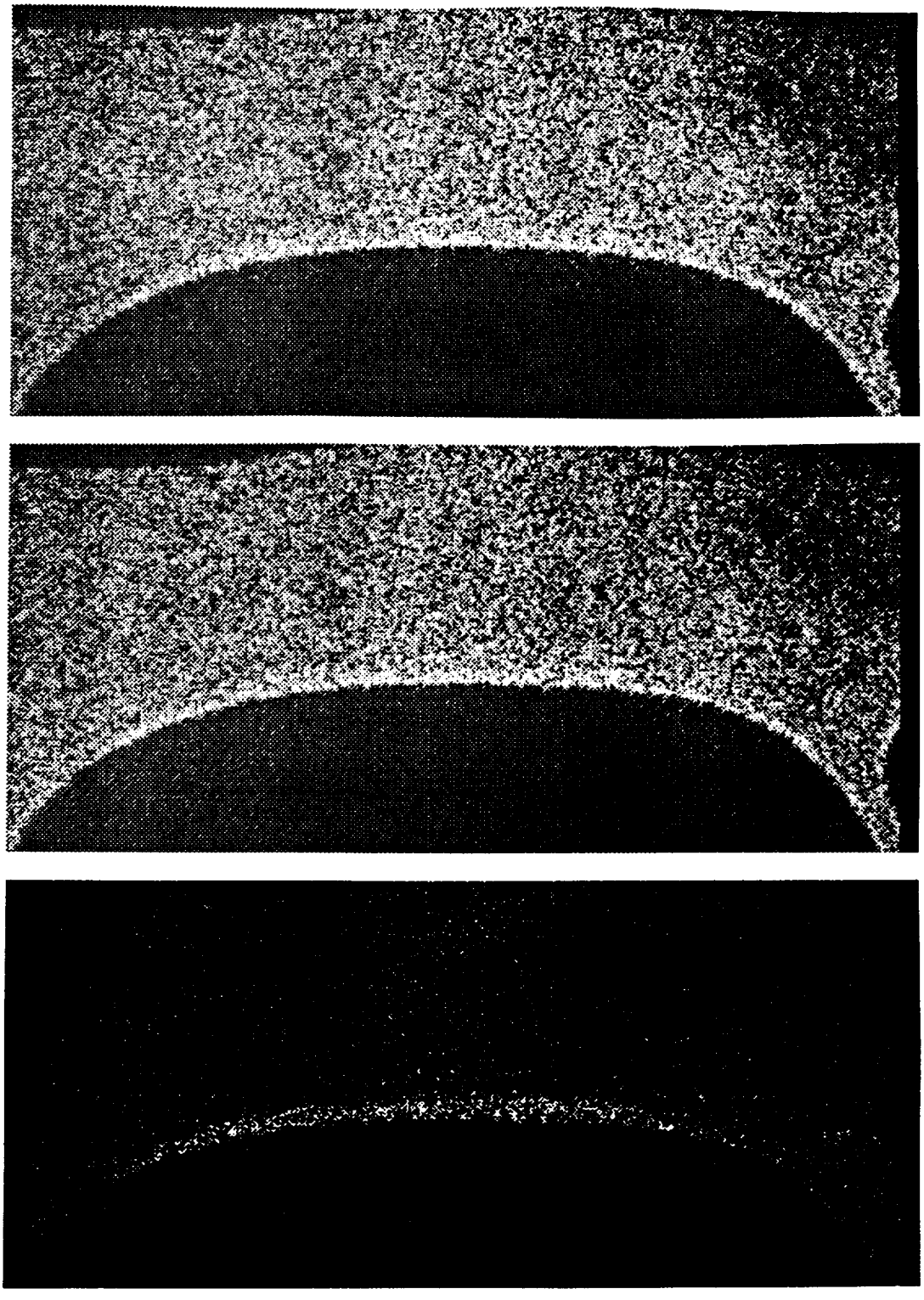

Figure 16. The speckle pattern analysis from the crystal growth cell (Hologram 2PO85 from the Spacelab III mission). **(a)** Original pattern, **(b)** pattern when the hologram is moved down by 0.1 mm, and (c) the subtraction of the intensities of the patterns of **(a)** and **(b)** above.

patterns locally are different and the subsequent substation still gives high contrast speckles. Away from the crystal surface in the fluid, both speckle patterns are more or less unchanged, so they yield to the minimum intensity in subtraction.

The present demonstration clearly shows the power of the speckle technique in holographic reconstruction. Digital image analysis, correlation studies, etc. can ultimately be utilized for quantitative applications.

6 CONCLUSIONS

Several important aspects of multi-color holography and speckle mode of analysis of holographic reconstructions have been covered in this report. The holographic fringe contrast in two-color holography with real crystal growth experiments has been considered in detail. Starting with the general mathematical relationships, the case of triglycine sulfate (TGS) aqueous solution has been discussed. With irrationally related wavelengths, although the holographic fringes change by introducing the test cell, the general conclusions on the fringe contrast remain unaffected. However, for frequency-doubled wavelengths, the advantages of phase control on the fringe contrast restricts to a smaller region of the hologram due to the crystal growth situation.

The proposed design concept of a three-color holographic system is basically that of introducing a third laser and related optics in the recently fabricated breadboard. This could be a logical first step in three-color holography.

Some prospective fluid and other types of experiments are also included in the report. It appears that the multi-color holography and interferometry can be useful in many new applications not necessarily limited to the traditional crystal growth situation.

Finally, the demonstration of a laser-speckle technique on the wave front reconstructed from a Spacelab III hologram clearly reveals the use in high refractive gradient situations. Traditional holographic interferometry gives very high frequency fringes in these situations. The speckle technique may provide useful data and the approach is of variable sensitivity.

In summary we have been able to refine several key aspects of multi-color holography. Also with demonstration of the speckle technique in this report and others earlier, the usefulness of unusual applications of holographic reconstructions is clearly established.

REFERENCES

1. C. S. Vikram, *Final Report*, Advanced Technology Development - Multi Color Holography, Contract No. NAS8-38609/D.O. No. 30, NASA George C. Marshall Space Flight Center, Huntsville, Alabama, January 1993.

2. C. S. Vikram, *Final Report*, Advanced Technology Development - Multi Color Holography, Contract No. NAS8-38609/D.O. 66, NASA George C. Marshall Space Flight Center, Huntsville, Alabama, January 1994.

3. C. S. Vikram, W. K. Witherow and J. D. Trolinger, Special beam intensity ratio needs in multi-color holography, *J. Mod. Opt.* **40**(7), 1378-1393 (1993).

4. C. S. Vikram, W. K. Witherow and J. D. Trolinger, Fringe contrast and phase effects in multi-color holography, *J. Mod. Opt.* **41** (8), 1531-1536 (1994).

5. R. C. Weast and S. M. Selby, Eds., Handbook of Chemistry and Physics, 48 th Edition, The Chemical Ruber Co., Cleveland, Ohio, 1967. p. E-160.

6. C. M. Vest, *Holographic Interferometry*, John Wiley & Sons, New York, 1979, p. 363.

7. R. L. Kroes and D. Reiss, Properties of TGS aqueous solution for crystal growth, *J. Crystal Growth* **69** (2/3), 414-420 (1984).

8. C. S. Vikram, W. K. Witherow and J. D. Trolinger, Determination of refractive properties of fluids for dual-wavelength interferometry, *Appl. Opt.* **31**(34), 7249-7252 (1992).

9. H. D. Yoo, W. R. Wilcox, R. Lal and J. D. Trolinger, Modelling the growth of triglycine sulfate crystals in Spacelab 3, *J. Crystal Growth* **92**, 101-117 (1988).

10. T. L. Spatz and D. Poulikakos, A two wavelength holographic interferometry study on the solidification of a binary alloy around a horizontal pipe, *Trans. ASME* **114**, 998-1010 (1992).

11. S. Hamid and R. P. Tatam, Simultaneous independent magnetic field and temperature measurement using optical interferometry, *Proc. SPIE* **1756**, 66-74 (1993).

12. P. B. Ruffin, C. Lofts, C. C. Sung and J. L. Page, Reduction of nonreciprocity noise in wound fiber optic interferometers, *Opt. Eng.* **33**, 2675-2679 (1994).

13. C. S. Vikram, Novel applications of speckle metrology, in *Speckle Metrology*, R. S. Sirohi (Ed.), Marcel Dekker, Inc, New York (1993), chap. 5.

14. Y. Song, Z. Guo, M. Groll and R. Kulenovic, Application of laser speckle photography in study of convective heat transfer, *Proc. SPIE* **2005**, 590-601 (1993).

15. K. Oberste-Lehn and W. Merzkirch, Speckle optical measurement of a turbulent scalar field with high fluctuation applications, *Experiments in Fluids* **14**(4), 217-223 (1993).

16. See for example, M Françon, *Laser Speckle and Applications in Optics*, Academic Press, Inc., New York (1979), Section 2.4.

NASA
National Aeronautical and Space Agency

Report Document Page

1. Report No.	2. Government Accession No.	3. Recipient's Catalog No.
Final		

4. Title and Subtitle

Development of Optical Systems

5. Report Due

01-08-1995

6. Performing Organization Code

University of Alabama in Huntsville

7. Aurthor(s)

Chandra S. Vikram

8. Performing Organization Report No.

Final

10. Work Unit No.

9. Performing Organization Name and Address

Center for Applied Optics
The University of Alabama in Huntsville
Huntsville, Alabama 35899

11. Contract or Grant No.

NAS8-38609, D.O. 110

12. Sponsoring Agency Name and Address

National Aeronautics and Space Administration
Washington, D.C. 20546-001
Marshall Space Flight Center, AL 35812

13. Type of report and Period covered

Final 03-09-1994 to 01-08-1995

14. Sponsoring Agency Code

15. Supplementary Notes

16.Abstract

Several key aspects of multi-color holography and speckle mode to study the holographic reconstructions are considered in the report. Holographic fringe contrast in two-color holography in the presence of a fluid cell in the object beam has been discussed in detail. Specific example of triglycine sulfate crystal growth situation is also considered as an example. A breadboard design using fiber optics and diode lasers for three-color holography for fluid experiments is presented. Possible role of multi-color holography in various new applications is summarized. Finally, the role of laser speckle technique is demonstrated for the study of holographic reconstructions. The demonstration is performed using a Spacelab III hologram.

17. Key Words (Suggested by Author(s))	18. Distribution Statement
Holography, three-colors, multi-colors, crystal growth, concentration, temperature, space applications, triglycine sulfate, Spacelab III, speckle, fringe contrast, refractive index, thermo-capillary phenomena, binary alloy, magnetic field, fiber optics, diode laser	

19. Security Class. (of this report)	20. Security Class. (of this page)	21. No. of pages	22. Price
Unclassified	Unclassified	30	

NASA FORM 1626 OCT 86